A geometric integration algorithm with applications to micromagnetics

D. Lewis* N. Nigam†

Abstract

The area of geometric integration theory can be employed when numerically solving an ODE or PDE with constraints. In this paper, we present an algorithm suitable for solving a PDE arising in micromagnetics with the property that the magnetic field consists at all times of unit vectors, and also include some comparisons with traditional methods of solving this system.

1 Introduction

In this set of notes, we describe a set of algorithms on multiple copies of S^2 (with possibly nonlinear interactions), with applications in material science. We begin by introducing a problem in micromagnetics and restating it in a setting where geometric integration methods may be applied. An arbitrary function appears in a family of geometric integration schemes for this problem; different choices of this function yield distinct discrete trajectories. We describe a possible choice that is related both to moving frames [13, 14, 23] and, in the case of a geometric version of the forward Euler method, to discretization error minimization. Work is in progress to identify analogous function choices for higher order methods [24, 23]. Finally, we present some representative numerical results that indicate that these geometric integration schemes are competitive with conventional numerical algorithms.

A promising area of application for such algorithms is numerical micromagnetics. Modern magnetic materials are used in an increasingly large number of applications, including thin film read heads and recording media [33], nanocrystalline permanent magnets, and magnetohydrodynamic fluids. In addition, there has been much interest in the use of "smart materials", including magnetostrictive actuators and organic ferromagnets [18]. These magnetic materials exhibit different responses corresponding to varying magnetic fields. For example, the resistance of a read-head ferromagnetic sensor changes as the device rotates over a recording medium. The magnetization of the material directly interacts with other physical and chemical characteristics, and micromagnetics is the theory that describes this

*Department of Mathematical Sciences, U. of California at Santa Cruz (lewis@math.ucsc.edu).
†IMA, U. of Minnesota, Minneapolis MN 55455 (nigam@ima.umn.edu).

interaction at a microscopic level. Of particularly great interest is the correlation of physical microstructure and magnetization; the ability to predict the response of one to variations in the other is crucial to the further development of these materials and devices.

Theoretical developments in micromagnetics are driven by industrial demands, and the need for accurate algorithms is now imperative. Conventional algorithms are still employed for highly sensitive calculations on large sensors, and are becoming increasingly inadequate. Moreover, the time-scales inherent in these problems vary from nano-seconds (in disk drives) to tens of seconds; hence integration techniques that remain effective over long times are required. An ideal integrator would resolve solutions accurately over very small time steps, while allowing large time steps to be taken when the system evolves over a long period.

At any point in time, the magnetization is typically constant in small regions in the material (termed domains), and the switching of these domains from one state to another is the basis of the functioning of devices built with these magnetic substances [10]. Ideally the entire device would be one large domain, which would switch instantaneously when an applied field was imposed. In practice, there are several domains, and the net magnetization in a desired direction is not optimal. We are interested in tracking the evolution of these domains, which entails following the local behavior of the magnetization. In industrial applications, a ferromagnetic device is subjected to changing magnetic fields (corresponding to the various applications — a disk moving underneath a read-head, changes in applied voltages for magnetorheological fluids, etc). One is interested in the response of the device to gradual changes in these external fields.

Another physical system whose mathematical model strongly resembles that of micromagnetics arises in the study of liquid crystals. Nematic and smectic liquid crystals form the basis of the operation of many every-day devices, such as LCD's, telecommunication devices, thermometers, projection systems — even mood rings. The devices operate on the principle that a suitable applied field will change the orientation of the liquid crystals, while conserving the pointwise-norm. Therefore, the resulting mathematical model has the same constraints as those in the micromagnetics situation. This system has been studied extensively, yet a norm-conserving algorithm has only been presented for an exceedingly simple situation [4].

2 A mathematical model of micromagnetics

A model that is widely used in industry is the *Landau-Lifshitz-Gilbert (LLG)* model of micromagnetics, which describes the evolution of the state of magnetization $\mathbf{M}$ in a ferromagnetic sensor, occupying a region $\mathcal{B}$ in space. The LLG equation for the magnetization $\mathbf{M}(x,t)$ is given by

$$\frac{\partial}{\partial t}\mathbf{M} = -\mathbf{M}\times H_{\text{eff}}(\mathbf{M}) - \lambda\mathbf{M}\times(\mathbf{M}\times H_{\text{eff}}(\mathbf{M})), \qquad \|\mathbf{M}(\mathbf{x})\| = 1 \ \ \forall\, \mathbf{x}\in\mathcal{B}. \tag{1}$$

Here λ is a damping parameter and H_{eff} is an effective magnetic field, described in detail below. The first term on the right hand side of (1) describes the (undamped) *Larmor precession* of $\mathbf{M}$ about H_{eff} and is derived from first principles [7, 2]. It is observed in physical experiments, however, that changes in magnetization decay in finite time. The second term

in (1) is a phenomenological term (called the *Gilbert damping term*, see [17, 21]), added to describe this damping behavior; it cannot be derived from first principles. There are situations under which this system is stiff (see, for example, [22]), and issues of numerical stability of the integration scheme are therefore important.

The effective field, which causes the magnetization to change, is derived from energy considerations [7], and varies nonlinearly with $\mathbf{M}$. More precisely,

$$H_{\text{eff}}(\mathbf{M}) = A \triangle \mathbf{M} + \mu_0 \left(-\nabla\phi + \mathbf{H}_{app}\right) + K(\mathbf{M}\cdot\mathbf{e})\mathbf{e}. \tag{2}$$

The parameters A and K are material constants of the permalloy being studied, and μ_0 is the permeability of free-space. The field $A \triangle \mathbf{M}$ is called the *exchange* field, preventing rapid spatial variations of $\mathbf{M}$ and the formation of arbitrarily fine domains (see [11, 36] for examples on how this term is computed in general). The next contribution in (2) is due to the nature of ferromagnetic crystals, which causes the magnetic moments to align in preferred directions. This effect is incorporated in the LLG model through the *uniaxial anisotropy* field $K(\mathbf{M}\cdot\mathbf{e})\mathbf{e}$. The external *applied field* is denoted by $\mathbf{H}_{app}$. The nonlinear, nonlocal contributions of $\mathbf{M}$ arise through the *demagnetizing field*, $-\nabla\phi$, where ϕ solves the Poisson problem with suitable boundary and radiation conditions

$$\triangle\phi = \nabla\cdot\mathbf{M} \qquad \text{in } \mathbb{R}^3;\ [\phi] = 0, \qquad \left[\frac{\partial\phi}{\partial n}\right] = \mathbf{M}\cdot\mathbf{n} \text{ on } \partial\mathcal{B}, \qquad \phi = o\left(\frac{1}{|x|}\right) \text{ as } |x|\to\infty. \tag{3}$$

Here $[u]$ denotes the jump of the function u across $\partial\mathcal{B}$. Many different methods exist for the calculation of this field, including the use of the full Maxwell system, FFT techniques, finite element methods, multigrid approaches, finite differences, and recently, fast multipole methods, [40, 32, 34, 38, 30, 1, 3, 6, 16, 28, 37, 15], among others. While there are still several unsettled issues in the area of demagnetizing field calculations (see [3] for a sharp critique on existing methods), it is not our intention in this project to duplicate this work. Instead, we shall focus on developing a time-stepping method that is robust, accurate, and requires relatively few field evaluations.

2.1 Why do we need geometric methods?

One of the intrinsic difficulties of the LLG model is that the magnetization $\mathbf{M}(x)$ only rotates; the point-wise norm of the magnetization is constant. However, a classical integrator will update the magnetization at time t to $\mathbf{M}(t+\triangle t)$ by the prescription

$$\mathbf{M}(t+\triangle t) = \mathbf{M}(t) + F(t, \triangle t, \mathbf{M}(t)).$$

The particular form of $F(\cdot,\cdot,\cdot)$ depends on the algorithm chosen; however, it is clear that all of these updates correspond to *translations* of $\mathbf{M}(t)$, not rotations. Thus, a classical integrator does not account for the fact that $\mathbf{M}$ evolves on a sphere. This constraint is difficult to efficiently impose in practice. A naive approach is to keep track of changes in the norm $\|\mathbf{M}(x,t)\|$ during a numerical experiment, and renormalize the iterates after a prescribed tolerance has been exceeded. However, this renormalization is equivalent to the

aphysical addition (or subtraction) of energy to the system and is therefore an undesirable solution.

Renormalizing $\mathbf{M}$ to conserve the norm while using conventional integrators changes the potential ϕ in a nonlinear fashion; it is easy to construct a simple example in which the renormalization introduces a significant change in the demagnetizing field. Assume that the magnetization $\mathbf{M}$ satisfies

$$\mathbf{M}(x, y, z) = a\,\mathbf{i} + b(x)\,\mathbf{j}, \tag{4}$$

for some constant a and scalar function b; here $\mathbf{i}, \mathbf{j}$ denote the usual unit vectors in the x and y directions. Before renormalization, the field $\mathbf{M}$ is divergence–free: $\nabla \cdot \mathbf{M} \equiv 0$. However, the renormalized field is *not* divergence–free:

$$\nabla \cdot \left(\frac{\mathbf{M}}{\|\mathbf{M}\|} \right) = -\frac{a\, b\, b'}{(a^2 + b^2)^{3/2}}.$$

The potentials obtained by solving (3) are clearly not the same for the original and renormalized fields. The effect of renormalization on the demagnetization field is particularly significant near domain boundaries. For example, if the function b appearing in (4) is a step function, then the divergence of the renormalized magnetic field is a delta function. We thank F. Reitich, [35], for this illustration of the dangers of normalizing vector fields.

Another difficulty arises due to the presence of multiple solutions. A ferromagnetic system seeks out energetically favorable states; however, there may be several states which are local minima of the energy [5, 29, 39]. We are interested in "neighboring" states — those that may not correspond to global energetic minima, but are minima the system settles into when the applied fields are perturbed slightly. Renormalizing the magnetization may force the system into different minima, thus changing the hysteretic characteristics. One may argue that a higher order integrator used with a much smaller time step, would introduce a smaller error in the norm. Unfortunately, this would require more function evaluations per time step, with each evaluation requiring a solution of the Poisson problem (3). This approach would significantly increase the computational expense.

A recent comparison of time-stepping algorithms employed in micromagnetics was presented in a review article [27], where the performance of various algorithms on two standard problems is compared. The striking message of the review was the lack of any one time-stepping method that would perform well on both standard problems.

The difficulties and costs involved in computing the demagnetization field while preserving the norm of the magnetization to high order make the LLG equation well–suited for geometric integrators, specifically the recently developed methods of symmetry-adapted numerical , schemes [8, 12], and geometric integration of ordinary differential equations on Lie groups, [25, 9, 19]. The underlying geometry of the micromagnetics problem motivates us to propose developing a numerical algorithm based on the Lie group of infinitesimal rotations. These algorithms can be used to modify existing integrators with little additional coding effort, and lend themselves to easy implementation.

3 Application of Lie group methods to micromagnetics

Numerical methods using geometrical techniques require an appropriate formulation of the problem. Prior to applying Lie group methods to the Landau-Lifshitz-Gilbert equation, we need to rewrite the LLG equation in terms of a transitive action of an appropriate Lie group on the manifold $\mathcal{M}$.

Recall that we have denoted the domain under consideration by $\mathcal{B}$. The configuration manifold $\mathcal{M}$ for the LLG system (1) is a homogeneous manifold on which the group $\mathcal{G}$ of smooth maps $\mathcal{Q} : \mathcal{B} \to SO(3)$ acts transitively, but not freely. Hence we can set $\mathbf{M}(x,t) = Q(x,t)\mathbf{M}_0(x)$ for some constant (with respect to time) unit vector field $\mathbf{M}_0$, and some time dependent curve $Q : \mathcal{B} \to SO(3)$. In the spatially discretized version of the system used in numerical simulations, suppose there are N grid points in space. We are interested in the evolution of $\mathbf{M}$ at these N points; we can view this as the motion of N 3-vectors, each moving on a copy of the sphere. Thus, the relevant manifold is the direct product $(S^2)^N$ of N spheres; the direct product group $\mathcal{G} = (SO(3))^N$ acts transitively on this manifold.

Let $\omega : \mathcal{M} \times \mathbb{R} \to \mathbb{R}^3$ denote the right trivialization of the time derivative of Q, i.e., the time dependent curve in the vector space $\mathcal{V}$ of maps from the sensor $\mathcal{B}$ to $\mathbb{R}^3$ satisfying $\dot{Q} = \text{skew}\,[\omega]\,Q$, where skew : $\mathbb{R}^3 \to so(3)$ satisfies skew $[\xi]\; x = \xi \times x$ for all ξ, $x \in \mathbb{R}^3$, and hence

$$\text{skew}\,[\xi] := \begin{pmatrix} 0 & -\xi_3 & \xi_2 \\ \xi_3 & 0 & -\xi_1 \\ -\xi_2 & \xi_1 & 0 \end{pmatrix}.$$

The LLG equation is then equivalent to the equations

$$\dot{\mathbf{M}} = \dot{Q}\mathbf{M}_0 = \text{skew}\,[\omega(\mathbf{M})]\,Q M_0 = \omega(\mathbf{M}) \times \mathbf{M} \tag{5}$$

and

$$\omega(\mathbf{M}) = \Xi(\mathbf{M}) + \sigma(\mathbf{M})\mathbf{M}, \qquad \text{where} \qquad \Xi(\mathbf{M}) = \lambda\,\mathbf{M} \times H_{\text{eff}}(\mathbf{M}) + H_{\text{eff}}(\mathbf{M}) \tag{6}$$

and $\sigma : \mathcal{M} \times \mathbb{R} \to \mathbb{R}$ is an arbitrary scalar function.

We can regard (6) as defining a family of ODEs

$$\dot{g} = \text{skew}\,[\omega(g \cdot \mathbf{M}_0)]\,g,$$

parametrized by $\mathbf{M}_0 \in \mathcal{M}$, on the group $\mathcal{G}$; in the discrete case, we can use the techniques developed for geometric integration on Lie groups to determine approximate discrete solution curves of these ODEs (see [25, 26, 31] and the references therein). Using the action of $\mathcal{G}$ on $\mathcal{M}$ to map these discrete trajectories in $\mathcal{G}$ onto $\mathcal{M}$ yields a geometric integration scheme for the discretized LLG system. Given a (right) trivialized ODE $\dot{g} = \xi(g)g$ on a Lie group G and an 'algorithmic exponential Exp : $\mathfrak{g} \to G$ approximating the true exponential map of G, an update of the form

$$g_{n+1} = \text{Exp}(\Delta t\,\xi_n)g_n$$

determines a one step method on G, where ξ_n is some approximation of $\xi(g_n)$ depending on g_n and the time step Δt. If G acts transitively on a manifold $\mathcal{M}$, then an ODE on $\mathcal{M}$ can

be expressed in the form $\dot{m} = (\tilde{\xi}(m))_{\mathcal{M}}(m)$, where $\tilde{\xi}_{\mathcal{M}}$ denotes the infinitesimal generator determined by $\tilde{\xi}$, with associated update

$$m_{n+1} = \mathrm{Exp}(\Delta t\, \tilde{\xi}_n) \cdot m_n.$$

For the rotation group $SO(3)$ both the true matrix exponential and the Cayley transform $\mathrm{cay}\,[\xi] = (I + \mathrm{skew}\,[\xi/2])(I - \mathrm{skew}\,[\xi/2])^{-1}$ can be efficiently evaluated and have frequently been used as algorithmic exponentials. (We identify the algebra $so(3)$ of $SO(3)$ with $\mathbb{R}^3$ using the map skew.) Here we use the Cayley transform, making use of the particularly simple expression

$$\mathrm{cay}\,[\nu]\,\mathbf{M} = \mathbf{M} + \frac{1}{1 + \|\nu/2\|^2}\left[-\nu \times \mathbf{M} + \frac{1}{2}\,\nu \times (\nu \times \mathbf{M})\right].$$

Thus we consider updates of the form

$$\mathbf{M}_{n+1} = \mathrm{Exp}(\triangle t\, \omega_n)\mathbf{M}_n, \tag{7}$$

where $\mathrm{Exp} : (\mathbb{R}^3)^N \to (SO(3))^N$ satisfies $(\mathrm{Exp}(\xi))_j = \mathrm{cay}\,[\xi_j]$.

Using (7), we now define one-step methods that are natural analogs of the standard explicit and implicit Euler methods:

$$\omega_n = \begin{cases} \Xi(\mathbf{M}_n) + \sigma(\mathbf{M}_n)\mathbf{M}_n & \text{forward Euler,} \\ \tilde{\Xi}(\mathbf{M}_n, \triangle t) + \tilde{\sigma}(\mathbf{M}_n)\mathbf{M}_n & \text{implicit Euler,} \end{cases} \tag{8}$$

where $\tilde{\Xi}(\mathbf{M}, \triangle t)$ denotes the solution of the implicit equation $\xi = \Xi(\mathrm{Exp}(\triangle t\, \xi)\mathbf{M})$ and the scalar functions σ and $\tilde{\sigma}$ are as yet unspecified.

The flexibility in the choice of map σ to be used in the update (7, 8) arises from the implementation of an update on a sphere using an update in the rotation group $SO(3)$, combined with the action of $SO(3)$ on the sphere. The three dimensional group $SO(3)$ acts transitively, but not freely, on the two dimensional sphere S^2; distinct ODEs

$$\dot{g} = \mathrm{skew}\,[\omega(g \cdot m_0)]\, g \qquad \text{and} \qquad \dot{g} = \mathrm{skew}\,[\tilde{\omega}(g \cdot m_0)]\, g,$$

where $\omega(m) - \tilde{\omega}(m) \in \mathrm{span}[m]$ for all $m \in S^2$, will typically have distinct solution curves in $SO(3)$, but the images in S^2 of those solution curves under the map $g \mapsto g \cdot m_0$ will coincide. We will discuss various approaches to the selection of the generator ω in the following sections, illustrating the general strategies with the help of two examples.

In section 6 we provide numerical results showing the effect of the parameter σ on the trajectories taken in case of the forward Euler algorithm. In particular, larger values of σ cause the trajectories to diverge sharply from those of the ordinary forward Euler; however, the final state is the same. A closer look at the equation shows that a larger value of σ corresponds to the inclusion of more precession in the trajectory. These numerical results clearly show that different choices of the parameter σ lead to significantly different numerical trajectories and thus motivate the search for an "optimal" value of σ. In section 4 we derive a choice of σ for the LLG equation that minimizes the discretization error for our geometric version of the forward Euler method. In section 5, we see that this choice can also be derived using a general geometric approach to generator selection. (See [24, 23] for descriptions of such approaches for more general manifolds.)

4 Numerical Micromagnetics: a forward Euler implementation

As was discussed in the previous section, the normal component of $\xi = \Xi(\mathbf{M})$ does not influence the solution curves of the original ODE. Thus, if we have a numerical algorithm of order n, this component does not affect the solution up to order n. However, it typically does appear in the higher order terms of the approximation, and theoretically a suitable choice of this component will reduce the discretization error. For the forward Euler scheme an optimal choice of σ, in the sense that this choice minimizes the discretization error, also has a natural geometric interpretation. Here we derive this map σ using a direct discretization error calculation; in the following section we shall discuss various geometric considerations that can be used in the selection of the generator to be used in a Lie group integration scheme.

We consider consistent algorithms using standard methods on the tangential component of ξ. The normal component is treated as a function of the tangential; we shall see that a component of the local discretization error at second order can be eliminated by a suitable choice of the normal component of the lowest order term in ξ.

We begin by examining the flow $\mathcal{F}_t$ of the ODE $\dot{\mathbf{M}} = \omega(\mathbf{M}) \times \mathbf{M}$ on $\mathcal{M}$ determined by a map ω satisfying $(\omega(\mathbf{M}))_j \in T_{m_j} S^2$ for $j = 1, \ldots, N$. The flow of this ODE satisfies

$$\mathcal{F}_t(\mathbf{M}) = \mathbf{M} + \triangle t\, \omega \times \mathbf{M} + \frac{\triangle t^2}{2} \left(\omega \times (\omega \times \mathbf{M}) + \dot{\omega} \times \mathbf{M}\right) + \mathcal{O}(\Delta t^2).$$

If the algorithmic update $\mathcal{F}_{\triangle t} : \mathcal{M} \to \mathcal{M}$, is given by

$$\mathcal{F}_{\triangle t}(\mathbf{M}) := \mathrm{Exp}\left(\triangle t\, \Xi(\mathbf{M}, \triangle t)\right) \cdot \mathbf{M},$$

where $\Xi(\mathbf{M}, \triangle t) := \sum_{j=0}^{\infty} \xi_j(\mathbf{M}) \frac{\triangle t^j}{(j+1)!}$ (note the nonstandard scaling of the coefficients in the expansion) and $\mathrm{Exp} : \mathbb{R}^3 \approx so(3) \to SO(3)$ agrees with the exponential map to second order (e.g. Exp is the Cayley transform), then

$$\begin{aligned}
\mathcal{F}_{\triangle t}(\mathbf{M}) &= \left(I + \triangle t\, \mathrm{skew}\left[\Xi\right] + \tfrac{1}{2} \triangle t^2 \mathrm{skew}\left[\Xi\right]^2 + \mathcal{O}(\Delta t^3)\right) \mathbf{M} \\
&= \left(I + \triangle t\, \mathrm{skew}\left[\xi_0\right] + \tfrac{1}{2} \triangle t^2 \left(\mathrm{skew}\left[\xi_1\right] + \mathrm{skew}\left[\xi_0\right]^2\right) + \mathcal{O}(\Delta t^3)\right) \mathbf{M} \\
&= \mathbf{M} + \triangle t\, \xi_0 \times \mathbf{M} + \tfrac{\triangle t^2}{2} \left(\xi_0 \times (\xi_0 \times \mathbf{M}) + \xi_1 \times \mathbf{M}\right) + \mathcal{O}(\Delta t^3).
\end{aligned}$$

The consistency condition for $\mathcal{F}_{\triangle t}$ is $\mathbb{P}_{\mathbf{M}} \xi_0 = \omega$. If $\mathcal{F}_{\triangle t}$ is consistent, then, setting $\sigma_0 := \langle \xi_0, \mathbf{M} \rangle$, the local discretization error is

$$\begin{aligned}
\frac{\mathcal{F}_{\triangle t}(\mathbf{M}) - \mathcal{F}(\mathbf{M})}{\triangle t} &= \tfrac{\triangle t}{2} \left(-\sigma_0 \mathbf{M} \times (\xi_0 \times \mathbf{M}) + (\xi_1 - \dot{\omega}) \times \mathbf{M}\right) + \mathcal{O}(\Delta t^2) \\
&= \tfrac{\triangle t}{2} \left(-\sigma_0 \omega + (\xi_1 - \dot{\omega}) \times \mathbf{M}\right) + \mathcal{O}(\Delta t^2).
\end{aligned}$$

The algorithm is thus second–order accurate iff

$$\langle \xi_1 - \dot{\omega}, \omega \rangle = 0 \qquad \text{and} \qquad \sigma_0 \langle \omega, \omega \rangle = \langle (\xi_1 - \dot{\omega}) \times \mathbf{M}, \omega \rangle. \tag{9}$$

In our geometric version of the forward Euler method, $\xi_j = 0$ for $j > 0$; thus this method will not be second order. However, we are free to choose σ_0 so as to satisfy the second equality in (9), e.g.

$$\sigma(\mathbf{M}, \Delta t) = \frac{\langle \Delta\omega(\mathbf{M}, \Delta t), \omega(\mathbf{M}) \times \mathbf{M} \rangle}{\|\omega(\mathbf{M})\|^2}, \tag{10}$$

where $\Delta\omega(\mathbf{M}, \Delta t)$ is some first order approximation to $\dot{\omega}(\mathbf{M})$ (e.g., a discrete difference approximation), yielding a discretization error–minimizing member of the family of algorithms (8).

This is a particular example of a more general result covering a large class of manifolds and higher order algorithms. (See [24, 23].) Work is in progress (Lewis, Nigam, Olver) to extend these or related results to an even larger class of systems, including the full discretized LLG system.

5 Generator selection — Expansions, curvature, and partial connections

A natural and obvious goal in selection of a numerical scheme is the achievement of the highest possible accuracy working within the given constraints. However, the prioritization of the constraints (efficiency, stability, developer effort, preservation of key features of the modeled system) can lead to significantly different approaches to the achievement of this goal and correspondingly different schemes. For the purposes of this discussion, we shall assume that we are given a family of one step methods of the form

$$(\mathbf{M}_{n+1})_j = \mathrm{Exp}(\triangle t\, \omega(\mathbf{M}_n, \Delta t)_j)(\mathbf{M}_n)_j \qquad j = 1, \ldots, N$$

for some map $\omega : (S^2)^N \times \mathbb{R} \to (\mathbb{R}^3)^N$ and some 'algorithmic exponential' $\mathrm{Exp} : \mathbb{R}^3 \to SO(3)$ satisfying $\mathrm{Exp}(0) = \mathbf{I}$, e.g. the matrix exponential or the Cayley transform.

We can optimize accuracy within this family of methods by selecting an appropriate generator ω; specifically, we shall first compute the update generator given some 'default' choice of generator, and then use that generator to determine an element of the isotropy algebra of the current state that minimizes the discretization error for that update. In the previous section we derived conditions specifying this choice of isotropy element for algorithms on $(S^2)^N$ utilizing the action of $(SO(3))^N$ using a traditional series expansion approach to the computation of the discretization error. (See [24] for the application of this approach and those discussed below to general homogeneous manifolds.) We now discuss some more geometric and, in some cases, less computationally intensive approaches to this task.

The geometric approach most closely related to the naive series expansion treatment is the use of geodesic curvature to characterize the essential information about curves on manifolds, e.g. solution curves of differential equations. A less directly related approach, but one that coincides with the direct error minimization approach for the forward Euler method on $(S^2)^N$, is the use of a partial moving frame and the associated partial connection form to determine a choice of generator. We shall define these constructions in section 5.3.

We first introduce some convenient notation and review some standard terminology from classical mechanics and dynamical systems theory. Let $\mathcal{M}$ be a manifold acted on by a Lie group G, with identity element e and Lie algebra $\mathfrak{g}$. Let $\Phi_g : \mathcal{M} \to \mathcal{M}$ and $\hat{\Phi}_m : G \to \mathcal{M}$ denote the maps

$$\hat{\Phi}_m(g) := \Phi_g(m) := g \cdot m$$

and let $\xi_{\mathcal{M}}$ denote the vector field $\xi_{\mathcal{M}}(m) := T_e\hat{\Phi}_m\xi$, called the *infinitesimal generator* associated to $\xi \in \mathfrak{g}$. The orbit $G \cdot m = \{g \cdot m : g \in G\}$ through $m \in \mathcal{M}$ has the tangent space

$$\mathfrak{g} \cdot m = T_e\hat{\Phi}_m \cdot \mathfrak{g} = \{\xi_{\mathcal{M}}(m) : \xi \in \mathfrak{g}\}\,.$$

The isotropy subgroup $G_m = \{g \in G : g \cdot m = m\}$ of a point $m \in \mathcal{M}$ consists of the group elements that fix m; the associated isotropy algebra is $\mathfrak{g}_m = T_eG_m = \ker[T_e\hat{\Phi}_m]$. The group action is said to be free if $G_m = \{e\}$ for every $m \in \mathcal{M}$.

5.1 Algorithms on S^2

To demonstrate the influence of the isotropy algebra on discrete trajectories, we first study the action of the rotation group $SO(3)$ on a single sphere S^2. Consider an autonomous vector field X on S^2 with flow $\mathcal{F}_t$. We will compare the performance of the forward Euler scheme with three different choices of generator for X, applying these schemes to the symplectically reduced rigid body equations. The first choice is a 'naive' or 'natural' one ω_n; for the rigid body system, this will be the body angular velocity. (For arbitrary vector fields X, there need not be a 'natural' choice; our intent here is to make a plausible choice of generator that one might make if the issue of isotropy were not taken into account.) The second choice is the orthogonal generator, i.e. the unique map $\omega_o\colon \mathcal{M} \to \mathbb{R}^3$ satisfying

$$X(m) = \omega_o(m) \times m \qquad \text{and} \qquad \langle \omega_o(m), m\rangle = 0$$

for all $m \in \mathcal{M}$. Our third choice improves the capture of the orbits by one order; for the forward Euler method, this choice will be second order accurate modulo time reparametrization. In the setting at hand, this choice has a particularly simple geometric interpretation, which we outline below.

A general and direct, but potentially computationally intensive, approach to the choice of a generator that reduces the discretization error is to compute the lowest order nonzero term in the series expansion for the discretization error for the family of algorithms under consideration, leaving the isotropy algebra component of the generator as an undetermined parameter, and thus determine conditions on the isotropy component that minimize the error. See [24] for a general treatment of this approach and section 4 for the derivation of the optimal generator choice for our forward Euler algorithm for the LLG system. for more detailed calculations for geometric integration schemes on homogeneous manifolds with nonfree group actions. Here we briefly explore some alternatives to this approach that have natural geometric interpretations.

If we assume that the algorithmic exponential is given by a rescaling of the matrix exponential (e.g. by the Cayley transform), then the update

$$m \mapsto \widetilde{\mathcal{F}}_t(m) = \exp(\tau(t, m)\,\omega(m)), \tag{11}$$

where τ is some unspecified rescaling of time, is given by a rigid rotation about an axis depending only on m. Hence the curve

$$\Gamma_\epsilon(m) = \left\{ \widetilde{\mathcal{F}}_t(m) : |t| \leq \epsilon \right\}$$

is a segment of a circle in S^2. Our goal is to choose the generator ω so as to obtain the best circular approximation at m to the true orbit segment

$$\mathcal{O}_\epsilon(m) = \{ \mathcal{F}_t(m) : |t| \leq \epsilon \} .$$

If $X(m) \neq 0$, then the optimal circular approximation to $\mathcal{O}_\epsilon(m)$ at m can be characterized using the geodesic curvature

$$k_g(m) = \frac{\langle (X \cdot \nabla) X(m), m \times X(m) \rangle}{\|X(m)\|^3}$$

of $\mathcal{O}_\epsilon(m)$ at m. The best circular approximation to $\mathcal{O}_\epsilon(m)$ at m is tangent to $X(m)$ at m and has geodesic curvature equal to that of $\mathcal{O}_\epsilon(m)$ at m. The first condition is clearly satisfied for any consistent update. The geodesic curvature $\tilde{k}_g(m)$ of $\Gamma_\epsilon(m)$ is easily seen to satisfy $|\tilde{k}_g(m)| = |\cot \phi|$, where ϕ is the angle between m and $\omega(m)$ (see, e.g. Do Carmo, p. 249); thus $|\tilde{k}_g(m)| = |\omega(m) \cdot m| / \|\omega(m) \times m\|$. Optimal orbit capture within the class of updates (11) is obtained using

$$\omega_c(m) := \omega_o(m) + k_g(m) \|X(m)\| \, m. \tag{12}$$

If $\mathcal{O}_\epsilon(m)$ is itself a segment of a circle, then ω_c yields $\Gamma_\epsilon(m) = \mathcal{O}_\epsilon(m)$. Hence any torsion–free orbits, e.g. the separatrices of the reduced rigid body equations, are captured exactly by this version of the Euler method. Note that the choice ω_o is suboptimal for the Euler method unless $k_g \equiv 0$ along the tractory of interest, i.e. unless the desired trajectory is a great circle.

For higher order methods, the axis of rotation used in the update map $\widetilde{\mathcal{F}}_t$ is typically time dependent and hence the corresponding algorithmic trajectory segment typically is not circular (i.e. it has nonzero torsion). Hence the simple argument used in the preceding paragraph cannot be applied. However, the strategy of curvature–matching can still be followed. Since a smooth curve on a two dimensional manifold in $\mathbb{R}^3$ is determined up to a time reparametrization by its geodesic curvature, we can determine the conditions on the generator imposed by the restriction that the geodesic curvature of $\widetilde{\mathcal{F}}_t(m)$ match that of $\mathcal{F}_t(m)$ to some order. The higher order derivatives of the curvature can either be determined analytically for a given vector field X or numerically approximated using standard difference schemes.

More generally, the choice a generator of a vector field on a homogeneous manifold can be viewed as a special case of the choice of a partial connection form, which generalizes to nonfree actions the classical connection form on a principal bundle. A partial connection form is a Lie algebra–valued one–form with appropriate equivariance properties. In section 5.3 we state the relevant definitions and present a family of partial connection forms on open subsets of S^2 that yield the discretization error–minimizing algorithm for the LLG given in section 4 and determine an algorithm that captures orbits to second order for any dynamical system on a single copy of S^2. The interested reader is referred to [23] for a more detailed treatment of partial connection forms and related constructions.

5.2 Application to the reduced free rigid body equations

We now apply the results outlined above to a simple and familiar system, the reduced rigid body equations on the sphere. Given a positive definite symmetric matrix $\mathbb{I}$, define the vector field

$$X(m) = m \times \mathbb{I}^{-1} m. \tag{13}$$

This is a Hamiltonian system with respect to the Kostant–Kirillov-Souraiu symplectic structure

$$\Omega(m)(\xi \times m, \eta \times m) = \langle m, \xi \times \eta \rangle$$

and Hamiltonian

$$H(m) = \tfrac{1}{2} \left\langle m, \mathbb{I}^{-1} m \right\rangle. \tag{14}$$

The system (13) is the symplectic reduction of the free rigid body equations on $T^*SO(3)$; more concretely, it is the restriction of Euler's equation for the body angular momentum to the unit sphere. (Since the norm of the body momentum is preserved by the dynamics of Euler's equation, all spheres centered at the origin are invariant submanifolds.) The conservative nature of this system makes it particularly easy to measure the error in orbit capture; if the body is triaxial, i.e. the eigenvalues of the inertia tensor I are distinct, the level sets of the Hamiltonian (14) exactly determine the orbits of the system. (If the body is axisymmetric, the 'equator' consists of fixed points; hence an energy–preserving scheme may allow drift across this family of one–point orbits.) Thus in this situation the error in the orbit is a function of the fluctuation in the energy.

Any map $\omega : S^2 \to \mathbf{R}^3$ of the form $\omega(m) = \mathbb{I}^{-1} m + \zeta(m)\, m$ for some scalar function $\zeta : S^2 \to \mathbb{R}$ is a generator of (13), i.e. $X(m) = \omega(m) \times m$. Hence any map of the form

$$\mathcal{F}_t^{\zeta}(m) = \mathrm{Exp}(\Delta t(\mathbb{I}^{-1} m + \zeta(m)\, m)) \cdot m,$$

where $\mathrm{Exp} : \mathbf{R}^3 \to SO(3)$ is some algorithmic exponential, can be seen as a version of the forward Euler method for (13). We consider the three generators

- $\omega_n(m) = \mathbb{I}^{-1} m$
- $\omega_o(m) = \mathbb{I}^{-1} m - \langle m, \mathbb{I}^{-1} m \rangle\ m$
- $\omega_c(m) = \mathbb{I}^{-1} m - \dfrac{\langle X(m), \mathbb{I}^{-1} X(m) \rangle}{\|X(m)\|^2}\, m = \mathbb{I}^{-1} m + \dfrac{\tau(u(m))}{\tau(\mathbb{I} u(m))}\, m,$

where $\tau : \mathbf{R}^3 \to \mathbf{R}$ and $u : S^2 \to \mathbf{R}^3$ are given with respect to an eigenbasis of $\mathbb{I}$ by

$$\tau(x) = x_1 + x_2 + x_3 \qquad \text{and} \qquad u(m)_i := (I_j - I_k)^2 I_i m_j m_k$$

for any cyclic permutation (i, j, k) of $(1, 2, 3)$. The first generator, ω_n, is the 'naive' choice; the second generator, ω_o, is orthogonal to the point of evaluation; the third generator, ω_c, captures orbits, and hence the energy, to second order.

As the numerical results given below demonstrate, the forward Euler scheme with generator ω_c yields an efficient, accurate algorithm for the reduced free rigid body. While the scheme captures orbits (and hence the energy) only to second order for asymmetric bodies,

the leading constants are quite small, yielding very good approximations even for very large time steps.

If the rigid body is axisymmetric, then all true trajectories consist either of equilibria (the 'poles' and the 'equator') or of steady rotations in the plane of symmetry. In this situation the forward Euler method with the generator ω_c associated to second order orbit approximation yields the exact solution when the true exponential map is used as Exp. (If the Cayley transform is used as the algorithmic exponential, then the orbits are captured exactly, but the algorithmic trajectories differ from the true trajectories by a time reparametrization.) Note that the 'naive' generator and the orthogonal generator yield only first order orbit approximations even in the axisymmetric case.

	ω_n	ω_o	ω_c
Triaxial	$6.37\ 10^{-2}$	$2.23\ 10^{-2}$	$4.60\ 10^{-6}$
Axisymmetric	$2.46\ 10^{-1}$	$1.46\ 10^{-1}$	$7.38\ 10^{-14}$

Table 1: Maximum energy error over the trajectories given in figure 1.

	Triaxial			Axisymmetric		
Δt	ω_n	ω_o	ω_c	ω_n	ω_o	ω_c
1	$2.58\ 10^{-2}$	$8.42\ 10^{-2}$	$1.69\ 10^{-4}$	$2.07\ 10^{-2}$	$5.27\ 10^{-2}$	$6.40\ 10^{-16}$
.1	$1.39\ 10^{-2}$	$1.25\ 10^{-2}$	$1.68\ 10^{-6}$	$3.29\ 10^{-3}$	$9.90\ 10^{-3}$	$8.38\ 10^{-15}$
.01	$1.33\ 10^{-3}$	$1.80\ 10^{-3}$	$1.67\ 10^{-8}$	$3.08\ 10^{-4}$	$8.73\ 10^{-4}$	$7.01\ 10^{-14}$

Table 2: Average maximum energy errors over ten sample runs with randomly generated initial conditions and inertia tensors, integrated over the interval [0, 100] using geometric versions of the forward Euler method. In all cases the Cayley transform was used as the algorithmic exponential.

In table 2 we provide the average maximum errors in the energy for time steps $\Delta t = 1$, .1, and .01, using for ten randomly generated initial conditions and inertia tensors each for triaxial and axisymmetric bodies.

As noted above, the separatrix is exactly captured if the generators ω_o or ω_c, which coincide on the separatrix, are used. On the other hand, when ω_n was used to integrate ten sample trajectories with initial conditions at random points on the separatrices of rigid bodies with randomly generated inertia tensors, the average errors over the integration interval [0, 500] were: $9.72\ 10^{-2}$ for $\Delta t = 1$, $3.89\ 10^{-2}$ for $\Delta t = .1$, and $1.94\ 10^{-3}$ for $\Delta t = .01$.

As implemented in our *Mathematica* code, the geometric version of the forward Euler method with orthogonal algorithmic velocity is approximately 10% slower than the naive version, while the version that captures orbits to second order is approximately 30% slower than the naive version.

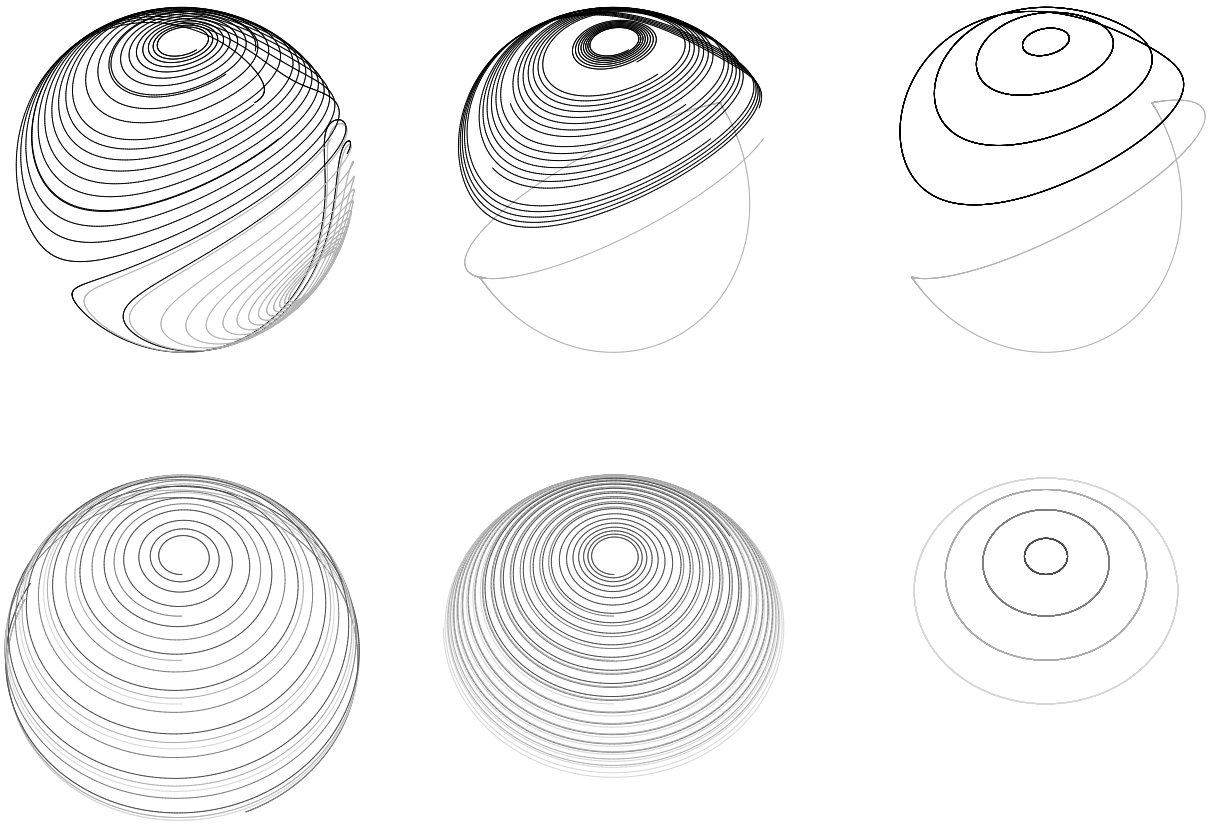

Figure 1: Sample trajectories computed over the interval [0, 200] using three geometric versions of the forward Euler method with the time step $\Delta t = 0.1$ and, left to right, the generators ω_n, ω_o, and ω_c. The upper row is computed using the inertia tensor of a trixial rigid body, while the lower row is computed for an axisymmetric rigid body. In all cases the Cayley transform was used as the algorithmic exponential.

We now consider four second order methods modeled on the classic Heun (RK2) method. In the first, we use the 'naive' generator $\omega_n(m) = \mathbb{I}^{-1}m$ in the Heun method, i.e.

$$\omega_n^{RK2}(m, \Delta t) := \tfrac{1}{2}\left(\omega_n(\mathrm{cay}\,[\Delta t\,\omega_n(m)]\,m) + \omega_n(m)\right) = \tfrac{1}{2}\mathbb{I}^{-1}(\mathrm{cay}\,[\Delta t\,\omega_n(m)]\,m + m);$$

the second method is entirely analogous, but with ω_n replaced with the orthogonal generator ω_o. In the third method, the infinitesimal rotation determined by applying the Heun method to the naive generator ω_n is modified by addition of an appropriate isotropy element to yield a higher order of orbit capture; specifically,

$$\omega_{nc}^{RK2}(m, \Delta t) := \omega_n^{RK2}(m, \Delta t) + \Delta t^3\,\sigma_n(m)m$$

where

$$\sigma_n(m) := \frac{\langle J^n, u\rangle}{\langle J^d, u\rangle}, \qquad \text{with} \qquad \begin{cases} u_j := (m_k m_\ell)^2 \\ J_j^n := -I_j(I_k + I_\ell)(I_k - I_\ell)^2 \\ J_j^d := 4\,I_1 I_2 I_3 I_j^2 (I_k - I_\ell)^2 \end{cases}$$

for any cyclic permutation (j, k, ℓ) of $(1, 2, 3)$. The fourth algorithm is analogous, but with ω_n^{RK2} replaced by ω_o^{RK2} and σ_n replaced by an appropriate function σ_o. (The function σ_o is a rational function in m and the components of the inertia tensor, but is significantly more complicated than σ_n.)

Although the Heun methods given here are only second order accurate, they capture the energy of the system to at least third order for any choice of isotropy element. The generators ω_{cn}^{RK2} and ω_{co}^{RK2} obtained by correcting the generators ω_n^{RK2} and ω_o^{RK2} using the isotropy maps σ_n and σ_o given above determine algorithms yielding at least fourth order energy capture for triaxial rigid bodies and fifth order energy capture for axisymmetric bodies. Running these algorithms on the randomly generated initial conditions and inertia tensors used in table 2, we obtain the average errors shown in table 3. Note that the corrected generators ω_{cn}^{RK2} and ω_{co}^{RK2} appear to yield fifth order global energy capture even for triaxial bodies. In fact, our numerical simulations using these generators show that the approximate trajectories oscillate about the correct energy level sets with a very slow average drift in the energy.

As implemented in our *Mathematica* code, the geometric version of the Heun method with orthogonal algorithmic velocity is approximately 10% slower than the naive version. The isotropy–corrected version of the naive version, with generator ω_{cn}^{RK2}, is is approximately 10% slower than the naive version, i.e. the same speed as the version with the orthogonal generator ω_o^{RK2}, while the isotropy–corrected version of ω_o^{RK2}, with generator ω_{co}^{RK2}, is approximately half the speed of the version with generator ω_o^{RK2}.

5.3 Partial connection forms

We now briefly discuss a general geometric approach to the selection of generators, using a generalization of the connection form on a principal bundle. For a more detailed treatment of partial connections and partial connection forms, and proofs of the assertions given below, see [23].

	Triaxial			
Δt	ω_n^{RK2}	ω_o^{RK2}	ω_{cn}^{RK2}	ω_{co}^{RK2}
1	$4.60\ 10^{-3}$	$6.23\ 10^{-3}$	$5.37\ 10^{-4}$	$1.03\ 10^{-3}$
.1	$5.27\ 10^{-6}$	$9.88\ 10^{-6}$	$7.34\ 10^{-9}$	$1.11\ 10^{-8}$
.01	$5.28\ 10^{-9}$	$9.90\ 10^{-9}$	$1.81\ 10^{-13}$	$1.29\ 10^{-13}$
	Axisymmetric			
Δt	ω_n^{RK2}	ω_o^{RK2}	ω_{cn}^{RK2}	ω_{co}^{RK2}
1	$5.46\ 10^{-3}$	$3.89\ 10^{-4}$	$2.08\ 10^{-4}$	$7.49\ 10^{-6}$
.1	$5.02\ 10^{-6}$	$3.89\ 10^{-7}$	$2.19\ 10^{-9}$	$7.54\ 10^{-11}$
.01	$5.02\ 10^{-9}$	$3.89\ 10^{-10}$	$1.01\ 10^{-13}$	$6.43\ 10^{-14}$

Table 3: Average maximum energy errors over ten sample runs with randomly generated initial conditions and inertia tensors, integrated over the interval [0, 100] using geometric versions of the Heun method. In all cases the Cayley transform was used as the algorithmic exponential.

We briefly review the fundamental properties of principal bundles and connections. (See, e.g., [20] for a detailed treatment of these topics.) A principal bundle is a quartet $(\mathcal{P}, \mathcal{B}, \pi, G)$ consisting of a manifold $\mathcal{P}$ with a free G action and a projection map $\pi : \mathcal{P} \to \mathcal{B}$ from $\mathcal{P}$ to the base manifold $\mathcal{B}$ such that $\pi(m) = \pi(\tilde{m})$ if and only if $\tilde{m} \in G \cdot m$, i.e. $\tilde{m} = g \cdot m$ for some $g \in G$, and $\mathcal{P}$ is locally trivial, i.e. every point $b \in \mathcal{B}$ has a neighborhood $\mathcal{U}$ such that $\pi^{-1}(\mathcal{U})$ is diffeomorphic to $\mathcal{U} \times G$. A *connection* on a principal bundle $\mathcal{P}$ is a distribution Γ satisfying

$$T_p\mathcal{P} = \mathfrak{g} \cdot p \oplus \Gamma_p \qquad \text{and} \qquad T_p\Phi_g \cdot \Gamma_p = \Gamma_{g \cdot p},$$

for all $p \in \mathcal{P}$ and $g \in G$. Specification of a connection Γ is equivalent to specification of an equivariant $\mathfrak{g}$–valued one–form α, called the *connection form*, satisfying

$$\alpha \circ T_e\hat{\Phi}_p = \mathrm{id}, \qquad i.e. \quad \alpha(p)(\xi_{\mathcal{P}}(p)) = \xi \qquad \text{for all } \xi \in \mathfrak{g},$$

for all $p \in \mathcal{P}$. By equivariance we mean that $\alpha \circ T\Phi_g = \mathrm{Ad}_g \circ \alpha$ for all $g \in G$. Here Ad_g denotes the adjoint action

$$\mathrm{Ad}_g\xi = \tfrac{d}{d\epsilon} g\, \exp(\epsilon\, \xi) g^{-1}|_{\epsilon=0}$$

of G on $\mathfrak{g}$. The connection Γ and connection form α are related by the condition $\ker[\alpha(p)] = \Gamma_p$ for all $p \in \mathcal{P}$.

The equivariance properties of connections and connection forms typically cannot be preserved in the context of nonfree actions, hence we relax these conditions, requiring only equivariance with respect to specified representatives of the isotropy equivalence classes. A map $\beta : G \times \mathcal{M} \to G$ is a *slip map* if $\beta(g, m) \cdot m = g \cdot m$ for all $g \in G$ and $m \in \mathcal{M}$. A (singular) distribution $\aleph$ assigning a complement $\aleph_m$ to $\mathfrak{g} \cdot m$ in $T_m\mathcal{M}$ for each point $m \in \mathcal{M}$ is a *partial connection* if there is a slip map β satisfying

$$T_m\Phi_{\beta(g,m)} \cdot \aleph_m = \aleph_{g \cdot m}$$

for all $g \in G$ and $m \in \mathcal{M}$. A *partial connection form* with slip map β is a $\mathfrak{g}$–valued one–form α on $\mathcal{M}$ satisfying

$$\alpha(m)(\eta_{\mathcal{M}}(m)) = \eta \mod \mathfrak{g}_m, \qquad \text{i.e.} \qquad T_e\hat{\Phi}_m(\alpha \circ T_e\hat{\Phi}_m - \mathrm{id}) = 0$$

and

$$\Phi^*_{\beta(g,m)}\alpha(m) = \mathrm{Ad}_{\beta(g,m)}\alpha(m) \mod \mathfrak{g}_{g\cdot m}$$

for all $g \in G$ and $m \in \mathcal{M}$.

If a group G acts transitively on a manifold $\mathcal{M}$, then every group orbit is equal to the entire manifold. In this situation, a (partial) connection form α assigns to each tangent vector a generator of that vector, so that

$$(\alpha(m)(\delta m))_{\mathcal{M}}(m) = \delta m$$

for all $\delta m \in T_m\mathcal{M}$ and all $m \in \mathcal{M}$. In particular, given a vector field X on $\mathcal{M}$, the map $\omega := \iota_X\alpha : \mathcal{M} \to \mathfrak{g}$, i.e. $\omega(m) = \alpha(m)(X(m))$, satisfies

$$\omega(m)_{\mathcal{M}}(m) = X(m)$$

for all $m \in \mathcal{M}$. Hence (partial) connection forms can be used to construct geometric integration schemes on manifolds with transitive actions. We are currently investigating the role of geometrically motivated choices of partial connection forms in the design of efficient geometric integration algorithms. As can be seen in the example discussed below, simple, natural choices of partial connection forms can lead to significant improvement in numerical performance.

One natural source of partial connections is a generalization of moving frames to manifolds with nonfree actions. In the modern sense, introduced by Fels and Olver [13, 14], a *moving frame* is a smooth equivariant map $\rho : \mathcal{P} \to G$ on a manifold $\mathcal{P}$ with a free group action. Recall that a principal bundle $\mathcal{P}$ is trivial if there exists a global section, i.e. a submanifold Σ of $\mathcal{P}$ such that each group orbit $G \cdot p$ in $\mathcal{P}$ intersects Σ exactly once. This condition corresponds to the existence of a moving frame. Specifically, given a global section Σ, for each point $p \in \mathcal{P}$ there is a unique group element $\rho(p)$ such that $\rho(p)^{-1} \cdot p \in \Sigma$; since the orbit $G \cdot p$ intersects Σ at eactly one point, we must have

$$\rho(p)^{-1} \cdot p = \rho(g \cdot p)^{-1} \cdot (g \cdot p),$$

which implies that the map ρ is equivariant, and hence a moving frame. On the other hand, if a moving frame $\rho : \mathcal{P} \to G$ is given, then the equivariance of ρ implies that the submanifold

$$\Sigma = \left\{\rho(p)^{-1} \cdot p : p \in \mathcal{P}\right\}$$

is a global section. A global section σ determines a flat connection, namely the connection that assigns to a point $p \in \Sigma$ the subspace $T_p\Sigma$ and assigns to any point $g \cdot p$ in the orbit of p the subspace $T_p\Phi_g \cdot T_p\Sigma$. (A flat connection is one with curvature identically equal to zero; for definitions of curvature, see, e.g. [20].) Given a map $\gamma : \mathcal{M} \to G$ and a tangent vector

$\delta m \in T\mathcal{M}$, the right trivialization of $T_m\gamma\,\delta m$ is an element of the Lie algebra $\mathfrak{g}$. Given such a map γ, we let $\tilde{D}\gamma : T\mathcal{M} \to \mathfrak{g}$ denote the map

$$\tilde{D}\gamma(\delta m) := T_m(R_{\gamma(m)^{-1}} \circ \gamma)\,\delta m$$

for any $m \in \mathcal{M}$ and $\delta m \in T_m\mathcal{M}$, where $R_g : G \to G$ denotes right multiplication by g. If ρ is the moving frame determined by a global section Σ, then the right trivialization $\tilde{D}\rho : \mathcal{P} \to \mathfrak{g}$ of ρ is the connection form of the connection determined by Σ.

Moving frames can be extended to manifolds with nonfree actions as follows: A (smooth) map $\phi : \mathcal{M} \to G$ is a (left) *partial moving frame* if

$$\phi_g(m) := \phi(g \cdot m)(\phi(m))^{-1} \tag{15}$$

satisfies

$$\phi_g(m) \cdot m = g \cdot m$$

for all $g \in G$ and $m \in \mathcal{M}$. A partial moving frame on a submanifold $\mathcal{S}$ of a manifold $\mathcal{M}$ with a G action is a map $\phi : \mathcal{S} \to G$ satisfying (15) for any $m \in \mathcal{S}$ and any $g \in G$ such that $g \cdot m \in \mathcal{S}$. The trivialized linearization $\tilde{D}\phi$ of a partial moving frame $\phi : \mathcal{M} \to G$ is a partial connection form, with associated slip map $\beta(g, m) = \phi_g(m)$. We refer to the trivialized linearization $\tilde{D}\phi$ as the partial connection form associated to the partial moving frame ϕ.

To illustrate the somewhat abstract geometric constructions described above, we now present a moving frame associated to the action of the rotation group $SO(3)$ on the unit tangent bundle $U(S^2)$ of the sphere S^2 and an associated family of partial moving frames on S^2. The partial connection form (which, in this case, is simply a map from the sphere to $\mathbb{R}^3$) of one of these partial moving frames yields the discretization error–minimizing generators used in the versions of the forward Euler method described in sections 4 and 5.2. As we shall see, this partial connection form and the associated generators can be derived without the use of the expansion of the discretization error.

The rotation group $SO(3)$ acts transitively on S^2 and freely and transitively on the unit tangent bundle $U(S^2) = \{u \in TS^2 : \|u\| = 1\}$. The map $\rho : U(S^2) \to SO(3)$ taking $u \in U_m S^2$ to the orthogonal matrix with columns $(m, u, m \times u)$ is a (left) moving frame with associated connection form

$$\tilde{D}\rho(\delta u) = m \times \delta m + \langle u \times \delta u, m\rangle\, m, \tag{16}$$

where $\delta u \in T_u U(S^2)$, with $m = \pi(u)$ and $\delta m = T_u\pi\,\delta u$. (Here $\pi : U(S^2) \to S^2$ denotes the canonical projection.) Note that we will regard u both as a tangent vector to the sphere at m and as a unit vector in $\mathbb{R}^3$.

Any unit vector field Y on a submanifold $\mathcal{M}$ of S^2 determines a partial moving frame $\phi = \rho \circ Y$ on $\mathcal{M}$, with partial connection form

$$\tilde{D}\phi(\delta m) = m \times \delta m + \langle Y(m) \times (DY(m) \cdot \delta m), m\rangle\, m. \tag{17}$$

The map ϕ_g associated to $g \in SO(3)$ is $\phi_g(m) = g\,\exp(\theta(g, m)\, m)$, where $\theta(g, m)$ denotes the angle between $g^{-1}Y(g\,m)$ and $Y(m)$. If the unit vector field Y is the normalization of a nonzero vector field X on some set $\mathcal{M} \subset S^2$, i.e. $Y(m) = X(m)/\,\|X(m)\|$, then (17) yields

$$\tilde{D}\phi(m)(\delta m) = m \times \delta m + \frac{\langle (\delta m \cdot \nabla)X, m \times X(m)\rangle}{\|X(m)\|^2}\, m. \tag{18}$$

In particular,

$$\tilde{D}\phi(m)(X(m)) = m \times X(m) + k_g(m)\ \|X(m)\|\, m, \tag{19}$$

where $k_g(\mathbf{M})(x)$ denotes the geodesic curvature of the curve $\mathbf{M}(x,t)$ in S^2.

The partial connection form (17) can be used to select the isotropy correction map (10) used in the micromagnetics algorithm. Following (19), we set

$$\tilde{\sigma}(\mathbf{M})(x) := \begin{cases} k_g(\mathbf{M})(x)\ \|X(\mathbf{M})(x)\| & X(\mathbf{M})(x) \neq 0 \\ 0 & X(\mathbf{M})(x) = 0 \end{cases}. \tag{20}$$

In our numerical implementation (10), we approximate $k_g(\mathbf{M})(x)$, using the identity

$$k_g(m) = \frac{\langle \ddot{m}, m \times \dot{m} \rangle}{\|\dot{m}\|^3} = \frac{\langle \dot{\omega}, \omega \times m \rangle}{\|\omega\|^3}$$

for a curve $m(t)$ in S^2 with nonzero velocity $\dot{m} = \omega \times m$, where ω is orthogonal to m, and replacing $\dot{m}$ and $\ddot{m}$ with finite difference approximations.

6 Numerical experiments using the first order integrator for the LLG equations

In this section, we describe a few experiments which were performed to examine the feasibility of using this geometric time-stepping method. Some of the results are shown in figures 2–6. In the experiments presented here, we use a one-dimensional ferromagnetic slab, with variations of $\mathbf{M}$ only along one direction. This enabled us to find an analytic expression for the demagnetizing field, which in turn helped us locate the exact solution of the (LLG) equation. In most applications, this option is not available to us; indeed, it is the lack of precise analytical results for comparison which makes numerical micromagnetics a challenging field. In our examples, we chose the largest possible time steps for a given method that would lead the system to the analytic solution (within prescribed tolerance).

We were particularly interested in the behavior of the free parameter σ which appears in the geometric time-stepping algorithm (6). Some of the key questions are:

- How do different choices of this parameter change the trajectory?
- If we compute the parameter using moving-frame theory, what path between the initial and final states does the integrator pick? Is there a natural manifold on which the LLG system evolves?
- How do choices of other variables such as strength of applied field, length of time step, and damping parameter, affect the parameter?

These experiments shed some light on all these issues, and encouraged us to pursue these experiments on larger, more realistic examples, which would include evaluations of the field as well.

As part of the numerical experiments, we studied the effect of choosing various parameters σ in a forward-Euler implementation of the LLG equation. We then tracked the evolution of

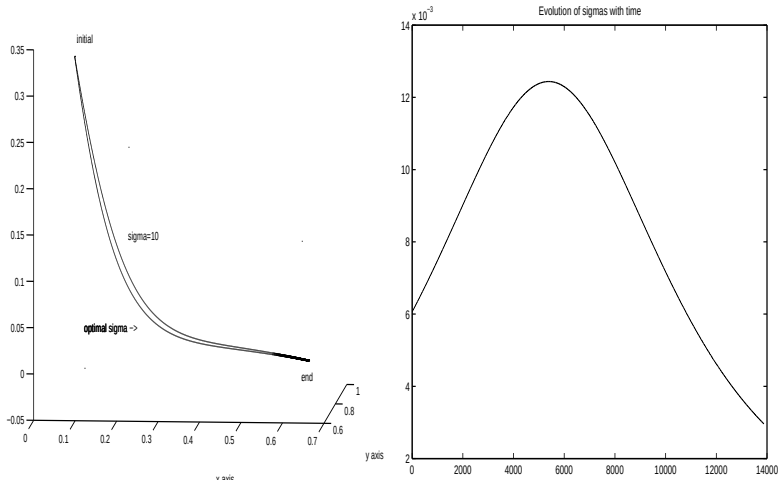

Figure 2: *The trajectories followed by the usual forward Euler* $\Delta t = 0.0001$ *and with the geometric forward Euler* ($\Delta t = 0.01$) *with optimal* σ *are almost identical; if we assume* $\sigma = 10$, *the trajectory precesses more before reaching the final point. The figure on the right shows the evolution of the optimal* σ. *The applied field is uniform and weak,* $\mathbf{H}_{app} = (0.05, 0.05, 0)$

the choice of σ given by (10). We approximated the acceleration $\ddot{\mathbf{M}}_n$ in (10) using a one-sided derivative of $\dot{\mathbf{M}}_n = X_n \times \mathbf{M}_n$. While most of the experiments involved the simplified LLG equation with no precession, we performed some experiments using the full LLG equations. The addition of the precession term typically leads to additional twisting of the trajectories; since the parameter σ was related to the curvature of the trajectory, we anticipated that it would change more when λ was nonzero. Our expectations were borne out by the numerical experiments.

Figures 2 and 3 describe the trajectories followed by the over-damped LLG system (without the Larmor precession term) for two different applied fields. We present, for comparison, trajectories computed using the usual forward Euler method with time step $\Delta t = 0.0001$, and the geometric forward Euler method with a much larger time step $\Delta t = 0.01$. Both trajectories end at the same final point. As we are only interested in the final equilibrium state of the system, we see the obvious merit of using the geometric integrator — we can obtain accurate final states while using much larger time steps.

We see the effect of varying the scalar functions σ on the trajectories. The effect is demonstrated clearly in figure 4, which depicts trajectories using different choices of σ. We notice certain trends in the function $\sigma(t)$ in figures 2, 3, 4, and we shall investigate the relationship of these trends to the physical processes occurring at the same times.

In figure 5, we implemented the code for the full LLG system, including the Larmor precession. The applied field is uniform, $\mathbf{H}_{app} = (5, 0, 0)$. The damping parameter λ was set to a low value, specifically $\lambda = 0.05$. The trajectories followed by the usual forward Euler $\Delta t = 0.0001$ and with the geometric forward Euler ($\Delta t = 0.01$) with optimal σ diverge appreciably, yet end at the same final state. The drift of the norm is now clearly visible (see figure (6)). The usual forward-Euler trajectory moves off the unit sphere, the geometrically integrated one does not. We see that the optimal σ now varies more (figure 5b).

To address the order of computational expense, we compared the geometric forward Euler

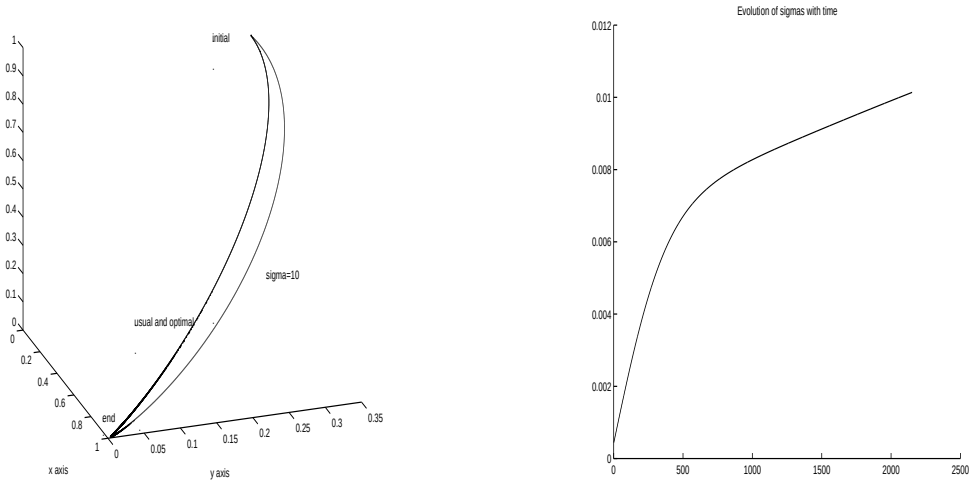

Figure 3: *The evolution of one point in the ferromagnetic sample. The trajectories followed by the usual forward Euler with time step* $\Delta t = 0.0001$ *and by the geometric forward Euler with optimal* σ *and time step* $\Delta t = 0.01$ *are almost identical; if we set* $\sigma \equiv 10$ *in the geometric forward Euler method, the trajectory precesses more before reaching the final point. The figure on the right shows the evolution of the optimal* σ*. The applied field is uniform,* $\mathbf{H}_{app} = (5, 0., 0)$

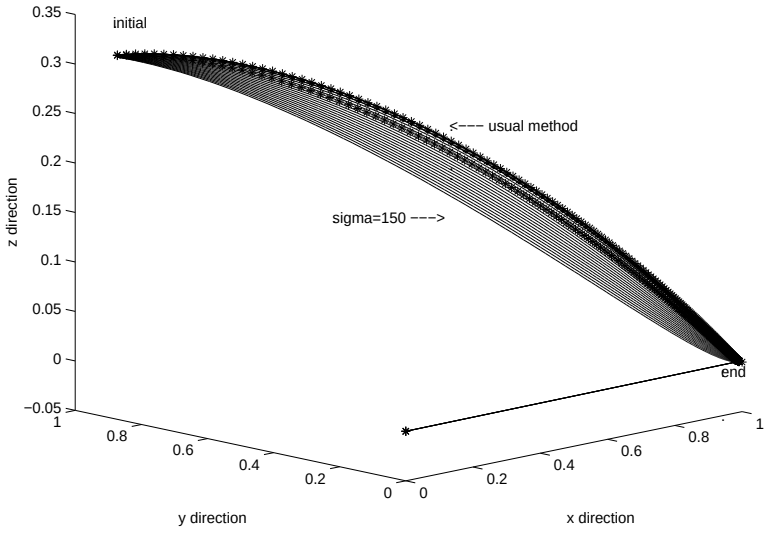

Figure 4: *This demonstrates the effect of choices of parameter* $\sigma(t)$ *on the trajectory. We picked* $\sigma(t)$ *to be various constants. The applied field was large,* $\mathbf{H}_{app} = (5, 0, 0)$*, and the example was run on the over-damped LLG. The trajectory that ends on the wrong final state corresponds to* $\sigma(t) = -20$*.*

method with time steps of $\triangle t = 0.01$ and 0.001 to the usual forward Euler with time step $\triangle t = 0.0001$. All final states corresponded to that computed by a fourth-order Runge-Kutta method with time step $\Delta t = 0.0001$, to within a relative error of 1%.

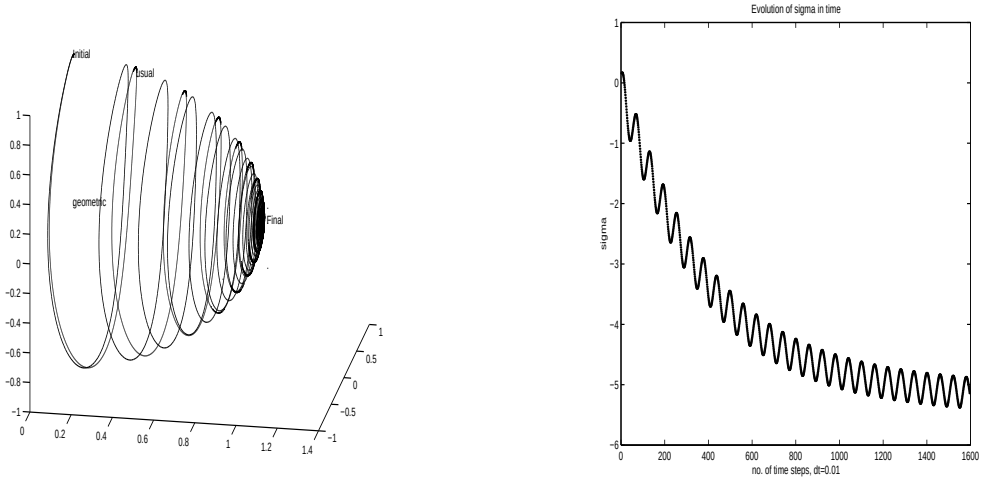

Figure 5: *An example with the full LLG system. Here the trajectory taken by the geometric method differs appreciably from those of the usual method, though the final state appears to be similar.*

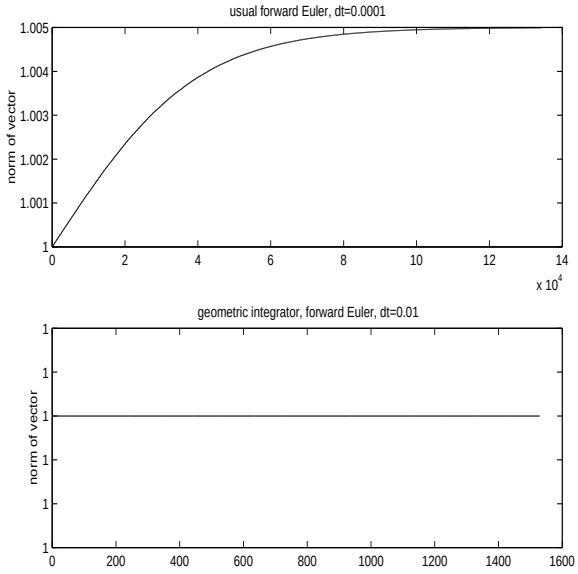

Figure 6: *Norm of magnetization in Fig(3). The geometric integrator exactly preserves the norm, even with a time step of* 0.01*. The usual forward Euler method shows a drift in norm, even with a time step of* 0.0001*.*

$\triangle t_{geometric}$	$cputime_{geometric}$	$cputime_{usual}$	Final $\|M_{geometric}\|$	Final $\|M_{usual}\|$
0.01	0.2100	3.8800	1.00000000	1.001183806
0.001	1.7700	3.8800	1.00000000	"

7 A higher order method for the LLG equation: RKMK4

In this section, we describe a fourth order Lie integrator for the LLG system. It is a modification of the standard RK4 method; a naive application of the usual RK4 method to the

generator ω fails to be fourth order accurate due to non-commuting flows. We have implemented the RKMK4 method [31], using the Cayley transform rather than the true matrix exponential. In common with the integrators decribed in the earlier sections, this algorithm conserves the norm of the magnetization to machine precision.

We begin with the Landau-Lifshitz-Gilbert equation for $\mathbf{M} := \mathbf{M}(t)$ in the form (5) and (6), with $\mathbf{M}(x,t) \in S^2$ for all x and t. To implement a Lie group integrator for (7) using the Cayley transform, we make use of the fact that for sufficiently small t, there is a function $f : \mathcal{B} \times \mathbb{R} \to \mathbb{R}^3$ satisfying

$$\mathbf{M}(x,t) = \mathrm{cay}\,[f(x,t)]\,\mathbf{M}(x,0). \tag{21}$$

Differentiating (21) with respect to t, we obtain

$$\begin{aligned}\dot{\mathbf{M}}(x,t) &= \mathrm{dcay}_f(f'(x,t)) \times \mathrm{cay}\,[f(t)]\,\mathbf{M}(x,t)\\ &= \mathrm{dcay}_f(f'(x,t)) \times \mathbf{M}(x,t)\\ &= \omega(\mathbf{M}(x,t))(x) \times \mathbf{M}(x,t),\end{aligned}$$

where the map $\mathrm{dcay}_f = \tilde{D}\mathrm{cay}(f) : \mathbb{R}^3 \to \mathbb{R}^3$ is the right trivialization of the tangent map of the Cayley transform. The initial condition for (21) is $f(0) = 0$.

Hence f' and ω are related by

$$\mathrm{dcay}_f(f'(t)) \times \mathbf{M}(t) = \omega(\mathbf{M}(t)) \times \mathbf{M}(t),$$

which is equivalent to

$$f'(t) = \mathrm{dcay}_f^{-1}(\Xi(\mathbf{M}(t)) + \zeta(t)\mathbf{M}(t)) \tag{22}$$

for some function ζ.

The map $\mathrm{dcay}_f : \mathbb{R}^3 \to \mathbb{R}^3$ satisfies

$$\mathrm{dcay}_f := \frac{1}{1 + \|\frac{1}{2}f\|^2}(I + \tfrac{1}{2}\mathrm{skew}\,[f]) \qquad \text{and} \qquad \mathrm{dcay}_f^{-1} = I - \tfrac{1}{2}\mathrm{skew}\,[f] + \tfrac{1}{4}ff^T. \tag{23}$$

The Cayley version of the RKMK4 method is essentially the conventional RK4 applied to (22): having found $\mathbf{M}_n$ at time t_n, we construct the update

$$\mathbf{M}_{n+1} = \mathbf{M}(t_n + \Delta t) = \mathrm{cay}\,[W]\,\mathbf{M}_n,$$

where

$$W = \tfrac{1}{6}(F_1 + 2F_2 + 2F_3 + F_4)$$

and

$$\begin{aligned} X_1 &= \Delta t\,\mathbf{X}(\mathbf{M}_n), & F_1 &= \mathrm{dcay}_{\mathbf{0}}^{-1} X_1\\ X_2 &= \Delta t\,\mathbf{X}(\mathrm{cay}\,[\tfrac{1}{2}X_1]\,\mathbf{M}_n), & F_2 &= \mathrm{dcay}^{-1}_{\frac{1}{2}X_1}(X_2)\\ X_3 &= \Delta t\,\mathbf{X}(\mathrm{cay}\,[\tfrac{1}{2}X_2]\,\mathbf{M}_n), & F_3 &= \mathrm{dcay}^{-1}_{\frac{1}{2}X_2}(X_3)\\ X_4 &= \Delta t\,\mathbf{X}(\mathrm{cay}\,[X_3]\,\mathbf{M}_n), & F_4 &= \mathrm{dcay}^{-1}_{X_3}(X_4). \end{aligned}$$

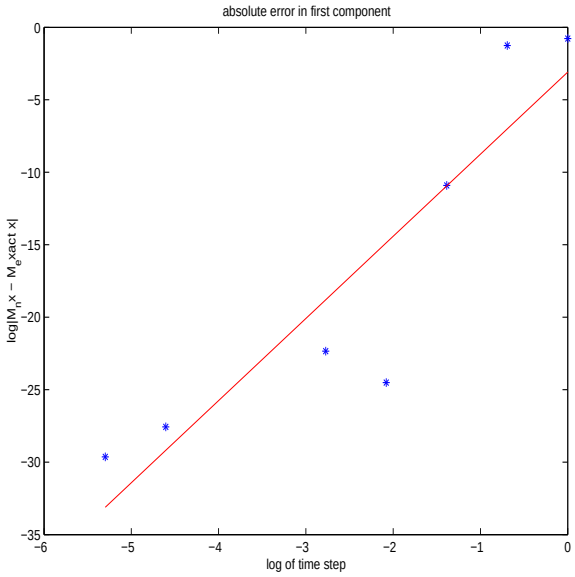

Figure 7: *Error in the first component of M as a function of time step. Here we see $O(\Delta t^{5.6})$ convergence.*

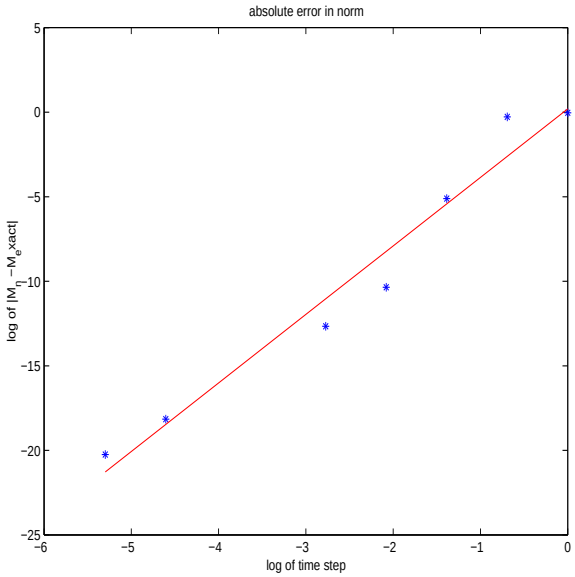

Figure 8: *Norm of the error of M as a function of time step. Here we see $O(\Delta t^{4.03})$ convergence.*

The Cayley analog of the RKMK4 method is fourth order accurate, as we have numerically verified for the LLG problem. (For simplicity, we tested only the case $\zeta \equiv 0$.)

The drift in the norm of $\mathbf{M}$ is zero up to machine precision. In figure 9 we track $\|\mathbf{M}\|$ over $[0, 1]$ with a time step of 0.01. The classical RK4 method without projection shows a drift in the norm; this drift is at 10^{-6}, ie, $O(\triangle t^3)$. The Lie group integrator, on the other hand, shows no drift (up to machine precision).

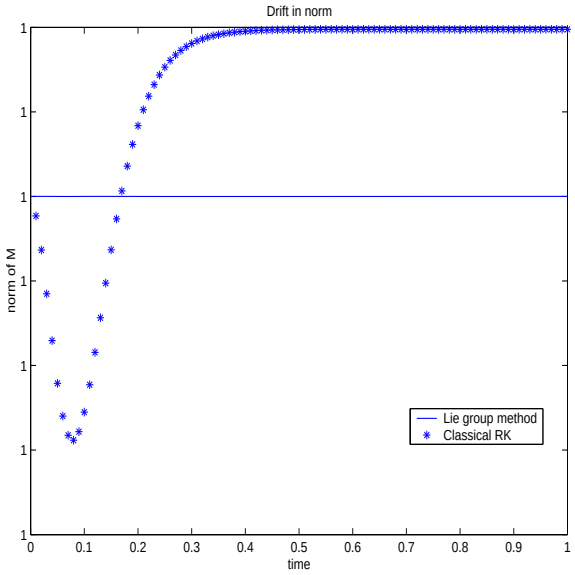

Figure 9: *The norm of the magnetization over the integration interval.*

References

[1] A. Aharoni, *Magnetostatic energy calculations*, IEEE Trans. Magnetics, 27 (1991), pp. 3537–3547.

[2] A. Aharoni, *Introduction to the theory of ferromagnetism*, in Monographs on Physics, Oxford University Press, 1996.

[3] A. Aharoni, *Crtitique on the numerical micromagnetics of nano-particles*, J. Magn. Mag. Mat., 203 (1999), pp. 33–36.

[4] F. Alouges, *A new algorithm for computing liquid crystal stable configurations: the harmonic mapping case*, SIAM J. Numer. Anal., 34 (1997), pp. 1708–1726.

[5] F. Alouges and A. Soyeur, *On global weak solutions for Landau-Lifshitz equations: existence and nonuniqueness*, Nonlinear Analysis, Theory, Methods and Applications, 18 (1992).

[6] P. Asselin and A. Thiele, *On the field lagrangians in micromagnetics*, IEEE Trans. Magnetics, 22 (1986), pp. 1876–1880.

[7] W. Brown, *Micromagnetics*, New York Interscience, 1963.

[8] C. Budd and C. Collins, *Symmetry based numerical methods for partial differential equations*, in Numerical analysis 1997, Longman, Harlow, 1998, pp. 16–36.

[9] C. Budd and A. Iserles, *Geometric integration: numerical solution of differential equations on manifolds*, Phil. Trans. Roy. Soc. London A, 357 (1999), pp. 945–956.

[10] B. Dieny, et al, *Magnetotransport properties of magnetically soft spin-valve structure*, J. Appl. Physics, 69 (1991), pp. 4774–4779.

[11] M. Donahue and R. McMichael, *Exchange energy representations in computational micromagnetics*, Physica B, 233 (1997), pp. 272–278.

[12] V. Dorodnitsyn, *Finite difference models entirely inheriting continuous symmetry of original differential equations*, Int. J. Mod. Phys. C, 5 (1994), pp. 723–734.

[13] M. Fels and P. Olver, *Moving coframes. i. a practical algorithm*, Acta Appl. Math, 51 (1998), pp. 161–213.

[14] M. Fels and P. Olver, *Moving coframes. ii. regularization and theoretical foundations*, Acta Appl. Math., 55 (1999), pp. 127–208.

[15] J. Fidler and T. Schrefl, *Micromagentic modelling of nanocrystalline magnets and structures*, J. Magn. Mag. Mat., 203 (1999), pp. 28–32.

[16] D. Fredkin and T. Koehler, *Ab initio micromagnetic calculations for particles*, J. Appl. Phys., 67 (1990), pp. 5544–5548.

[17] T. Gilbert, *A lagrangian formulation of gyromagnetic equation of the magnetization field*, Phys. Rev., 100 (1955).

[18] A. Iraqi, et. al., *Functionalisation of poly(p-phenylenevinylene) polymers with pendant nitroxide groups"*, Synthetic Metals, (1997).

[19] A. Iserles, H. Munthe-Kaas, S. Norsett, and A. Zanna, *Lie group methods*, Acta Numerica, (2000), pp. 215–365.

[20] S. Kobayashi and K. Nomizu, *Foundations of Differential Geometry*, vol. I, Interscience Publishers, 1963.

[21] L. Landau and E. Lifshitz, *On the theory of magnetic permeability in ferromagnetic bodies*, Physik. Z. Sowjetunion, 8 (1935).

[22] D. Lewis and E. Della Torre, *Identification of stiff modes in micromagnetics problems*, IEEE Trans. Magn., 33 (1997), pp. 1596–1599.

[23] D. Lewis, N. Nigam, and P. Olver, *Connections for nonfree group actions.* Preprint, 2001.

[24] D. Lewis and P. Olver, *Geometric integration algorithms on homogeneous manifolds.* Preprint, 2001.

[25] D. Lewis and J. C. Simo, *Conserving algorithms for the dynamics of Hamiltonian systems on Lie groups*, J. Nonlinear Sci., 4 (1994), pp. 253–299.

[26] ——, *Conserving algorithms for the n dimensional rigid body*, Fields Institute Communications Series, 10 (1996), pp. 121–139.

[27] L. Lopez-Diaz, J. Eicke, and E. Della Torre, *A comparison of micromagnetic solvers*, IEEE Trans. Magnetics, 35 (1999), pp. 1207–1210.

[28] M. Luskin and L. Ma, *Numerical optimization of the micromagnetics energy*, in Proceedings of the Session on Mathematics in Smart Materials, SPIE 1993 Conference on Smart Structures, 1993.

[29] W. Miranker and B. Willner, *Global analysis of magnetic domains*, Quart. of Appl. Math, (1979), pp. 219–238.

[30] P. Monk and O. Vacus, *Accurate discretization of a nonlinear micromagnetic problem.* June 1999.

[31] H. Munthe-Kaas, *Runge-kutta methods on lie groups*, BIT, 38 (1998), pp. 92–111.

[32] J. Oti, *Numerical micromagnetic techniques and their applications to magnetic force microscopy calculations*, IEEE Trans. Magnetics, 29 (1993), pp. 2359–2364.

[33] S. Parkin, *The magic of multilayers*, Tech. Rep. 1, IBM, 1998. Vol 42.

[34] S. Polstyanko, G. Peng, and J.-F. Lee, *Algebraic multigrid method for solving FEM matrix equations for 3d static problems*, IEEE Trans. Magnetics, 35 (1999), pp. 1183–1186.

[35] F. Reitich. private communication, Dec 1999.

[36] W. Scholz, *Micromagnetic simulation of thermally activated switching in fine particles*, PhD thesis, Institut fur Angewandte und Technische Physik der Technischen Universitat Wien, 1999.

[37] T. Schrefl and J. Fidler, *Numerical micromagnetics in hard magnetic and multilayer systems*, J. Appl. Phy., 79 (1996), pp. 6458–6463.

[38] I. Tsukerman, *Fast finite element solvers for problems with magnetic materials*, IEEE Trans. Magnetics, 29 (1993), pp. 2365–2367.

[39] A. Visintin, *On Landau-Lifshitz' equations for ferromagnetism*, Japan J. Appl. MAth., 2 (1985), pp. 69–84.

[40] B. Yang and D. Fredkin, *Dynamical micromagnetics by the finite element method*, IEEE Trans. Magnetics, 34 (1998), pp. 3842–3852.